Since January 2020 Elsevier has created a COVID-19 resource centre with free information in English and Mandarin on the novel coronavirus COVID-19. The COVID-19 resource centre is hosted on Elsevier Connect, the company's public news and information website.

Building and Environment 206 (2021) 108280

Contents lists available at ScienceDirect

Building and Environment

journal homepage: www.elsevier.com/locate/buildenv

Implication of coughing dynamics on safe social distancing in an indoor environment—A numerical perspective

Jayaveera Muthusamy [a,*], Syed Haq [a], Saad Akhtar [b], Mahmoud A. Alzoubi [c], Tariq Shamim [d], Jorge Alvarado [e,a]

[a] Department of Mechanical Engineering, Texas A&M University, College Station, TX, USA
[b] Department of Mining and Materials Engineering, McGill University, Montreal, QC, Canada
[c] Department of Mechanical Engineering, Université de Sherbrooke, Sherbrooke, QC, Canada
[d] Department of Mechanical Engineering, Northern Illinois University, DeKalb, IL, USA
[e] Department of Engineering Technology and Industrial Distribution, Texas A&M University, College Station, TX, USA

ARTICLE INFO

Keywords:
Coughing evolution
Computational Fluid Dynamics
Lagrangian modeling
Contamination range
COVID-19
Face mask efficacy

ABSTRACT

Coughing is a primary symptomatic pathway of respiratory or air-borne disease transmission, including COVID-19. Several parameters such as cougher's age, gender, and posture affect particle dispersion indoors. This study numerically investigates the transient cough evolution, contamination range, particle reach probability, and deposition fraction for different age groups of males and females in standing and sitting postures in a ventilated room. The efficacy of a cloth mask has also been studied with and without the influence of air ventilation. Validated Computational Fluid Dynamics methodology has been implemented to model complex physics such as turbulent buoyant cloud, particle–air interaction, particle collision/breakup, and droplet evaporation. Our results show that overall, the contamination range is slightly lower for females due to lower cough velocities and particle counts. Moreover, a significant fraction of particles crosses the two meters social distancing guideline threshold with an unhindered cough. Besides, wearing a cloth mask reduces the average contamination range by approximately two-third of the distance compared to coughing without the mask. However, aerosolized particles reach longer streamwise distances and drift for extended durations beyond thirty seconds. This study can be used to improve the heating, ventilation, and air conditioning recommendations and distancing guidelines in indoor settings.

1. Introduction

The recent outbreak of COVID-19 has resulted in a catastrophic impact on the human condition. The respiratory illness has not only resulted in infecting over 140 million people to date, but it has also adversely affected the global economy by limiting the mobility of over 50% of humankind [1]. Due to several factors such as the lesser understood mutability of the virus, the contagious asymptomatic period, and its human-to-human transmission mechanisms, it is imminent to investigate the factors that govern the spread of the virus exhaustively. Several pathways have been identified for the spread of COVID-19, amongst which the airborne transmission was found, in particular, to be virulent, even more so than transmission due to contaminated surfaces and animal-to-human contact [2,3]. According to several recent studies [4–8], poor ventilation standards were found to be a critical factor in outbreaks of the virus in indoor spaces. Thus to characterize the contaminant spread in the indoor spaces, it is essential to understand the mechanisms by which the infectious particles can spread from the source to the surroundings [9]. This will lead to a better understanding of the transmission mechanisms and help policymakers and government officials make informed decisions about social distancing.

Coughing has been demonstrated to cause a significant efflux of pathogens from the infected transmitter [10–13]. A single cough can contain over 75,000 particles only in aerosols (<10 [μm]) [14]. Numerical modeling, and experimental fluid pattern studies have been used to gain more insights into the coughing dynamics to study the spread of viral outbreaks (Severe Acute Respiratory Syndrome, Middle Eastern Respiratory Syndrome) and to understand the virus' transmission [15–18]. The literature clearly shows that human cough is one of the main sources of spreading virus-borne nuclei from a symptomatic source. The violent expiratory event in the form of a cough results in the emission of droplet sizes ranging between 5 [μm]–1000 [μm], following roughly a log-normal distribution [12]. Furthermore, the velocity field

* Corresponding author.
E-mail address: jayaveera@AggieNetwork.com (J. Muthusamy).

https://doi.org/10.1016/j.buildenv.2021.108280
Received 29 April 2021; Received in revised form 17 August 2021; Accepted 18 August 2021
Available online 30 August 2021

Nomenclature

$\dot{m}_p$	Mass transfer rate of the particle [kg/s]
$\dot{m}_{pi}$	Mass transfer rate of an individual component, i [kg/s]
$\hbar$	Heat transfer coefficient [W/(m^2 K)]
Re_p	Reynolds number of the particle [-]
$\mathbf{f}_d$	Drag force [N]
$\mathbf{f}_d$	Gravitational force [N]
$\mathbf{f}_d$	Pressure force [N]
$\mathbf{g}$	Gravitational acceleration [m/s^2]
A	Surface area of particle [m^2]
B	Spalding transfer number [-]
C_d	Drag coefficient [-]
d_i	Distance traveled by the particle from the mouth [m]
g^*	Mass transfer conductance [kg/(m^2 s)]
h	Enthalpy [J/kg]
k	Thermal Conductivity [W/(m K)]
m_p	Mass of particle [kg]
N_i	Cumulative number of particles deposited [-]
n_p	Number of particles in a cell of continuous phase [-]
N_t	Total number of particles deposited [-]
p	Pressure [N/m^2]
S_c	Two-way coupling source term in the momentum equation [N/m^3]
S_t	Two-way coupling source term in the energy equation [W/m^3]
T	Temperature [°C]
U	Velocity of the fluid [m/s]
v_p	Particle velocity [m/s]

Greek Symbols

Δt	Time step size [s]
δt_p	Dirac delta function [-]
ε_i	Fractional mass transfer rate of each component [-]
ρ	Density of fluid [kg/m^3]

of these particles also follows a distribution with a peak value of up to 11 [m/s] [19]. This implies that it is important to characterize the cough dynamics rigorously in order to develop accurate models that can capture the droplet dispersion. A vast literature of experimental and numerical studies exists on characterizing the human cough [20–23]. In an experimental and computational study by Zhang et al. [24], a thorough characterization of the cough dynamics was undertaken where an experimental simulator was designed to replicate the actual behavior of the mucus spray. The dispersion of the atomized droplets was numerically evaluated using Lagrangian mechanics in a flow field pre-determined by simulations. Recently, Bi [25] studied the dispersion of the human cough jet development using the Lagrangian–Eulerian method in a quiescent environment. The study also investigated the droplet dynamics using the Discrete Particle Modeling (DPM) approach. The droplet size distribution was found to have a key role in airborne and droplet transmission. Diameters less than 10 [μm] were observed to be suspended rather easily in the ambient air resulting in airborne transmission. The ambient Relative Humidity (RH) and inlet cough velocity were also observed to impact the penetration distance of the droplet and thus affecting the transmission process. Similar conclusions were drawn in other studies, which investigated the effects of ventilation on the indoor spread of COVID-19. Bhagat et al. [26] examined the role of ventilation on COVID-19 spread through theoretical and practical fluid mechanics considerations. Their analysis concluded that while ventilation has its trade-off in terms of balancing energy efficiency and minimizing the exposure risk to contaminants, it does play a critical role in the spread of COVID-19. They also concluded that displacement ventilation effectively reduces exposure risk since it encourages vertical stratification and is designed to remove the polluted warm air near the ceiling.

Numerical investigation of the bio-contaminant spread and risk of infection due to coughing in different indoor environments has been a subject of several studies in the literature. In a study, Zhang et al. [27] numerically investigated the droplet dispersion from coughing and breathing in a ventilated room. The study used Large Eddy Simulation to model the carrier phase and DPM for the particles. The model was used to evaluate ten different cases with three levels of RH, ventilation rate, and ambient temperature. Another study by Zhu et al. [28] investigated the infection through saliva droplets dispersed by coughing. Lagrangian tracking of the droplets emitted from three different subjects was simulated in different room-types, occupant postures, and location of the diffusers. They discovered that the droplets with diameters less than 30 [μm] were dispersed in the air, and the risk of inhaling was strongly influenced by the relative positioning of the air-conditioning diffuser and the occupant. Another recent study by Chen et al. [29] investigated the highest exposure risk of respiratory infection when a healthy person was in proximity of an infected person. They reported that the short-range airborne sub-route dominates the close contact transmission and that smaller droplets are more prone to follow the indoor air stream.

In addition to the droplet velocity and diameter distributions, another crucial characteristic of a typical cough event is the formation of turbulent buoyant clouds that result from it [21,30,31]. This localized turbulent puff has implications in suppressing the local evaporation rates from the sputum, which the coughing modeling methodology should consider explicitly. A study by Li et al. [32] implements a multi-component Eulerian-Lagrangian approach to model evaporation and dispersion of the cough droplets in the quiescent environment. Their study concluded that the heterogeneous humidity field strongly affected the characteristics of droplet evaporation. Wei et al. [11] numerically investigated the effect of turbulence fluctuations of the cough jet on the dispersion of droplets. Turbulence fluctuations were found to substantially impact the prediction of both the streamwise and lateral spread of the particles for different size ranges. The study also showed that aerosols and large particles were mildly affected by the change in the ambient RH, whereas the medium-sized particles (diameter of 30 [μm]) evaporated instantly.

While significant progress in mathematical and computational studies has been made to model the effects of cough dynamics on contaminant spread, there are still many open questions in the literature that need to be addressed. These questions can be broadly categorized into two themes, mainly (i) Validity of the model assumptions, and (ii) Simulation scenarios. Regarding model assumptions, the majority of the literature studies simplify the coughing dynamics by using average velocity and mono-dispersed particle sizing for coughing. Further, the complex momentum and mass interactions between the turbulent cough cloud and the surrounding air are often neglected. Regarding the simulation scenarios, to the best of our knowledge, no study in the literature has reported or shown how different combinations of age, gender, postures, face mask usage, and ventilation could affect the contamination range. This study aims to address these limitations by developing a 3-D computational model that considers the turbulence of the cough jet, intricate evaporation patterns, and detailed cough dynamics. It also presents a wide range of scenarios involving different age groups, gender, ventilation, and postures. Appropriate parameters such as contamination range, PRP, and deposition fraction are

mathematically defined, and the computational data from numerical simulations are quantitatively and qualitatively analyzed using these parameters.

This paper is structured as follows. Section 2 discusses the theoretical model development outlining the assumptions, governing equations, and boundary conditions that form the basis of this study. Section 3 presents the details of the numerical solution and the validation results with experimental results available in the literature. This is followed by a detailed discussion on the parametric study results as shown in Section 4, where the effects of age, gender, posture, and ventilation conditions on the airborne particulate transmission when mask and no mask cases are presented. Finally, relevant conclusions are drawn in Section 5 to elucidate the effects of different parameters evaluated in the results section on contaminant spread. Lastly, areas of study are laid out for future work direction.

2. Model development

2.1. Problem statement

This study investigates coughing pattern inside an air-conditioned room, as shown in Fig. 1 (a). The room is ventilated using displacement ventilation with ceiling supply and return. The person is assumed to be standing or sitting directly underneath the supply vent. A single cough is modeled for all cases with an average coughing time set at 0.5 [s]. The particle size distributions (size and count of particles) coming out of the mouth for each gender and age group are defined, based on data available in literature [20]. Each particle is modeled so that it consists of 93.5% water and 6.5% non-evaporative components [33]. As it is shown later, after an expiratory event, heavier particles start moving towards the ground while smaller particles rise due to buoyancy. Furthermore, particle coalescence and breakup produce a wide range of particle sizes. After a single coughing event, the spread and reach of particles are observed and measured for 30 [s]. The case of male less than thirty (M < 30) is defined as a base-case. This scenario is further modeled taking into account when a cloth mask is worn. Additionally, the effect of air-conditioning stream on particle dispersion is also investigated.

2.2. Governing equations

A Lagrangian–Eulerian coupled method is used in this study. The Lagrangian method is implemented to track the path of each particle in the cough cloud. In addition, the Eulerian approach is used to simulate the coughing behavior inside an air conditioned room. The two-way coupling aims to incorporate the effect of the airflow on the cough particle dispersion and vice-versa. The mass and momentum conservation equations are divided into two categories as follows.

— Continuous Phase (Eulerian):

Mass and momentum conservation equations used in the simulations are obtained by ensemble averaging the instantaneous momentum equation. With compressible flow conditions assumed, these equations are represented in gradient form as:

$$\frac{\partial \rho}{\partial t} + (\nabla \cdot \rho \mathbf{U}) = 0 \tag{1}$$

$$\frac{\partial (\rho \mathbf{U})}{\partial t} + \nabla \cdot (\rho \mathbf{U} \otimes \mathbf{U}) = -\nabla p + \rho \mathbf{g} + \mu \nabla^2 \mathbf{U} + S_c \tag{2}$$

where S_c includes source terms to model body force and Lagrangian coupling. In present study, Sc is the source term for coupling Lagrangian phase (droplets) with Eulerian phase (air), which is shown in Eq. (8). For modeling turbulence within the domain, the realizable k-ε method is used [34]. This eddy viscosity model utilizes a two-layer approach, which allows the k-ε model to be applied in the viscous-affected layer (including the viscous sub-layer and the buffer layer). Furthermore, the k-ε model has two additional transport equations for turbulence kinetic energy and energy dissipation rate. The k-ε model has a wide range of applications and has been employed in several similar studies [28,35,36].

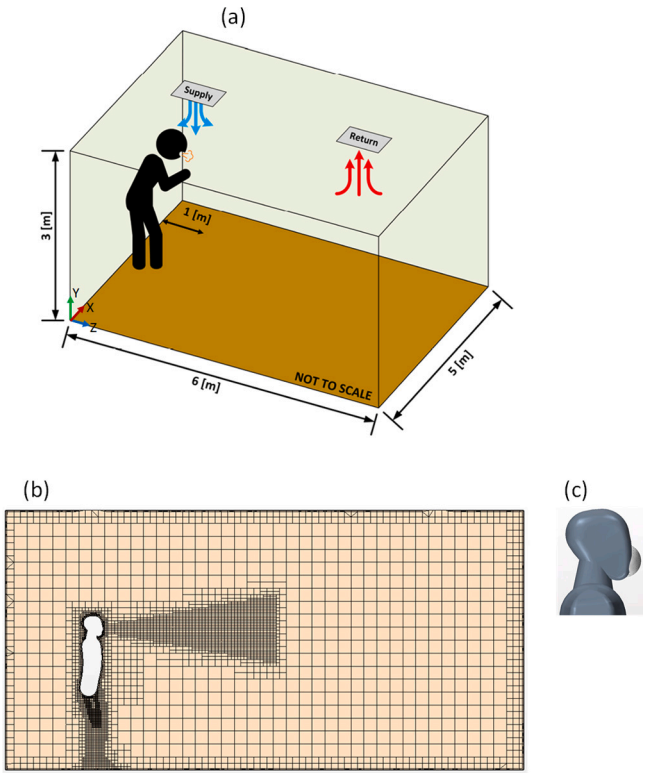

Fig. 1. Illustration of the (a) computational domain of the indoor space with ceiling ventilation (b) computational grid of the cross-sectional area in the Y–Z plane, and (c) mask model on the mannequin's face.

A coupled solution approach for energy is employed in this study. The energy is represented as:

$$\left[\frac{\partial (\rho h)}{\partial t} + \nabla \cdot (\rho h \mathbf{U})\right] = \nabla \cdot (k \nabla T) + S_t \tag{3}$$

where h is the enthalpy of the fluid and S_t is the source term from the Lagrangian phase convective heat transfer applied in the continuous phase energy equation.

— Discrete Phase (Lagrangian):

Discrete phase modeling is performed by tracking each particle of a multi-component fluid. For each particle, the conservation equations of momentum are applied as follows:

$$m_p \frac{d \mathbf{v}_p}{dt} = \mathbf{f}_d + \mathbf{f}_p + \mathbf{f}_g \tag{4}$$

where m_p and $\mathbf{v}_p$ are the mass and velocity of the particle and $\mathbf{f}_d$, $\mathbf{f}_p$, and $\mathbf{f}_g$ are drag, pressure and gravitational forces acting on the particle, respectively.

Particles in turbulent flow are exposed to a randomly-fluctuating velocity field corresponding to their inertia. To account for this behavior, turbulence dispersion force is simulated by a stochastic method that incorporates the influence of instantaneous velocity variations on the particles. The Eulerian phase turbulence model (k-epsilon) provides the time scales and length of the turbulent eddies that are formed and the fluctuating velocity field on the particles are then applied until the eddy interaction time is surpassed. Hence, the instantaneous fluid velocity using Reynolds Averaged Navier–Stokes equations is used to estimate the slip-velocity and employed to Lagrangian phase models using particle Reynolds number.

The drag force, $\mathbf{f}_d$ in Eq. (4), is modeled using the following equation:

$$\mathbf{f}_d = \frac{1}{2} C_d \rho A \left(\mathbf{U} - \mathbf{v}_p\right) \tag{5}$$

where C_d is the drag coefficient of the particle and ρ is the density of the continuous phase. C_d based on the particle Reynolds number (Re_p) is calculated using the Schiller–Naumann correlation [37], which is stated as:

$$C_d = \begin{cases} \frac{24}{\mathrm{Re}_p}\left(1 + 0.15\mathrm{Re}_p^{0.687}\right), & \mathrm{Re}_p \le 10^3 \\ 0.44, & \mathrm{Re}_p > 10^3 \end{cases} \tag{6}$$

Energy conservation equation for the discrete phase is stated as:

$$m_p C_p \frac{dT_p}{dt} = S_t \tag{7}$$

The effects of continuous phase on the discrete phase is also accounted for by enabling two-way coupling between Eulerian (air) and Lagrangian (droplets) phases. For an unsteady coughing process, the rate of momentum transfer from all particles in a cell, c, to the continuous phase is modeled using a source term in the continuous phase momentum equation, as follow:

$$S_c = -\frac{1}{\Delta t} n_p \left[\left(\mathbf{f}_d + \mathbf{f}_p\right) + \dot{m}_p \mathbf{v}_p\right] \delta_{tp} \tag{8}$$

where Δt is the time step size of the continuous phase, n_p is the number of particles in a cell of continuous phase while $\dot{m}_p$ is the mass transfer rate to the particle. The convective source term in the energy equation is given by $S_t = f\hbar A_s(T - T_p)$ where $\hbar$ is the heat transfer coefficient, A_s is the particle surface area and f is the mass transfer correction from El Wakil [38].

At the scale of cough particles, several phenomena take place simultaneously, including droplet collision, breakup, and evaporation. Therefore, particle collision is simulated using the No Time Counter Collision Model [39], which predicts the probability of two particles colliding. Once the collision occurs, it is modeled based on the following outcomes; bounce, permanent coalescence, reflexive separation, and stretching separation (grazing collision). The outcome is determined using Weber number and a collision regime map. Particle breakup is accounted using Kelvin–Helmholtz Rayleigh–Taylor particle Breakup model [40]. This model uses shear and acceleration instabilities to simulate the droplet breakup.

Evaporation of the cough particles is taken into account from the mass transfer of liquid species from the discrete to the continuous phase. For this purpose, discrete and continuous phases are modeled as multi-component fluid mixtures. The composition of cough droplet is determined using the methodology introduced by Lui et al. [33]. It is assumed that the droplet consists of 93.5% evaporative, aqueous solution and 6.5% non-evaporative components. The latter includes all mucous organic compounds and glycoproteins. A typical cough particle at ambient condition loses the evaporative component if the relative humidity (RH) is lower than a threshold value of 67% [33], depending upon the partial and saturation pressures. Specifically, the water evaporates resulting in the formation of a crust surrounding the periphery of the pre-existing droplet. This crust, composed of lipid monolayers, prevents the remaining liquid from being evaporated. Thus the diameter of the subsequent particle is assumed to be the nuclei diameter. The volume fraction occupied by these insoluble components is calculated to be 6.5%.

Particle evaporation is simulated using the quasi-steady multi-component droplet evaporation model [41]. The evaporative mass transfer rate is computed by using the expression:

$$\dot{m}_{pi} = -\varepsilon_i g^* A_s \ln(1 + B) \tag{9}$$

where ε_i is the fractional mass transfer rate of each component, g^* is mass transfer conductance, A_s is the surface area of the particle, and B is the Spalding mass transfer number. The definition of these parameters depends on the mode of evaporation. In this study, the vapor diffusion limited evaporation mode is implemented to simulate the particle evaporation [41]. Spalding number is also used, which is the ratio of mass fraction of the liquid at the droplet surface to the mass fraction of the liquid in the free stream. Physically, it is the driving force for mass transfer. The mass transfer conductance is a function of the molecular diffusivity and the particle Sherwood number that is defined based on the Ranz–Marshall correlation [42].

2.3. Computational domain and boundary conditions

The computational domain of an air-conditioned room is used in this study, as depicted in Fig. 1 (a). The dimensions of the floor are 5 × 6 [m], while the height of the room is 3 [m]. Two ceiling ventilation vents are introduced to the domain with identical dimensions of 0.2 × 0.2 [m]. The mannequin of the coughing person is placed directly beneath the supply vent. The height of the person is chosen based on the nominal heights of North American males and females. For standing posture, the average male and female heights are 1.77 [m] and 1.62 [m], respectively [43]. For sitting posture, on the contrary, the mouth is positioned approximately 0.3 [m] (1 [ft]) lower than at the standing posture. The opening of the mouth is modeled as a circle with a cross-sectional area of 4.00 [cm^2] for male and 3.37 [cm^2] for female [19]. Moreover, a cloth mask with an average pore size of 4 [μm] is modeled in this study. Since the cloth masks do not perfectly fit a typical face, a 2[mm] gap is assumed between the face and the mask [44]. The mask follows the contour of the face, with 2 [mm] offset from the human face surface, thus ensuring a uniform gap. This is illustrated in Fig. 1 (c).

The computational domain, comprising of the mannequin and the room, was discretized using an unstructured-type, hexahedral, cut cell mesh elements. The mesh insensitivity study was undertaken and the node count of 288,420 cells was found to yield a good balance between the computational speed and numerical accuracy. Additional information on the grid independence study is provided in Appendix A. The grid in the coughing cloud region as shown in Fig. 1 (b), was refined to capture the dynamics of the turbulent jet accurately. The time step size for both Eulerian and Lagrangian (discrete) phase analysis was kept at 0.001 [s] with maximum sub-steps of 2000,000 for the particle phase.

The velocity profile shown in Fig. 2 is used as a boundary condition to simulate the air coming out of the mouth during the coughing event. The transient coughing velocity profile is generated using different mouth opening area and flow rates for males and females from the literature [19]. The velocity profile of the cough differs between males and females; however, the overall trend is the same, as illustrated in Fig. 2. Similarly, the particle diameters during a coughing instance vary from 0.3 to 55 [μm] based on the gender and the age of the person [20]. To represent these factors, each gender is divided into three age groups [20]. The total number of particles expelled from each gender and age group is shown in Table 1. The particle size distribution and the velocity trends are used as inlet boundary conditions set at the mouth. It is worth mentioning here that in all cases, the total time of a single cough lasted 0.5 [s] [43]. The droplets of each size are continuously released at every time-step for the duration of coughing event i.e. 0.5 [s]. The initial velocity of the droplets are same as the time dependent velocity (Fig. 2) of the air coming out of the mouth [19]. The velocity of the airflow from the supply vent is set at 3.53 [m/s]. The selection of this velocity is based on the criteria of average Air Change per Hour (ACH) of approximately 5. This value is the average ventilation rate for typical office buildings given by American Society of Heating Refrigerating and Air-Conditioning Engineers (ASHRAE) Standard 62.1 [45] and ASHRAE Standard 55 [46]. The boundary conditions at the supply and return vents are inlet velocity and pressure outlet, accordingly. The walls are assumed to be non-slip type boundary condition.

Table 1
Discrete particle distribution for different age groups (male and female [20])

Particle diameter [μm]	Age ≤ 30		30 < Age ≤ 50		Age > 50	
	Male	Female	Male	Female	Male	Female
0.30	5.22×10^7	2.09×10^7	2.07×10^7	6.87×10^7	1.62×10^8	6.48×10^7
0.75	7.42×10^5	9.66×10^5	7.18×10^5	1.59×10^6	1.06×10^6	8.83×10^5
1.75	1.35×10^5	4.40×10^4	7.10×10^4	1.66×10^5	1.13×10^5	1.55×10^5
5.75	1.57×10^5	4.87×10^4	6.99×10^4	1.86×10^5	1.74×10^5	1.77×10^5
55.0	7.30×10^3	1.94×10^3	3.03×10^3	1.30×10^4	1.31×10^4	1.06×10^4

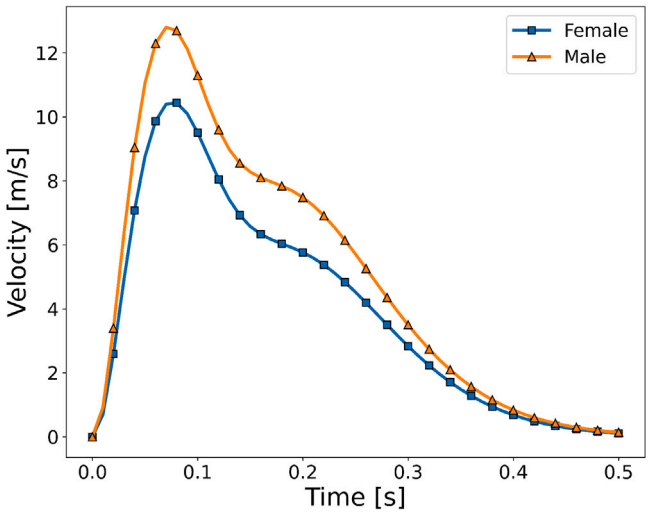

Fig. 2. Average coughing velocity profile for male and female. After Gupta et al. [19].

The supply inflow air temperature and humidity are set as 23 [°C] and 45%, respectively. The human body surface temperature is fixed at 37 [°C] in all the simulations while the human skin is assumed to be an impermeable surface. The buoyancy effects in the vicinity of the human body are considered negligible since the Richardson number ($Ri = Gr/Re^2$) was computed to be less than 0.1 under all physical conditions for this study. The temperature and humidity of exhaled air are set as 35 [°C] and 85% . In addition, the temperature and humidity of the room are initialized at 23 [°C] and 45%, respectively.

The effect of cloth masks on the spread of particles is also studied. The cloth mask is modeled using an isotropic porous medium in the domain [47]. The resistance offered by the mask to the flow of air is modeled using Darcy–Forchheimer equation. This equation provides the viscous and inertial permeability coefficients derived from the velocity and pressure drop experimental data of the cloth mask [44,48]. The permeability coefficients resulting in the inertial ($P_i = 6.35 \times 10^6$ [kg/m^4]) and viscous resistance ($P_v = 2.04 \times 10^6$ [$kg/(m^3\ s)$]) of the cloth mask are calculated from the experimental values of pressure drop and velocity from Saldaeva [48]. A Lagrangian filter is applied to the inlet surface of the porous medium to filter out particles larger than 4 [μm].

In this study, fifteen cases are simulated in total as outlined in Table 3. These include six standing cases for each gender and age group, followed by six sitting cases. The age groups are divided into three main categories: less than 30 years, from 30 to 50 years, and older than 50 years. An additional case is simulated to determine the effect of lack of air condition ventilation on the spread of particles, followed by another case that examines the effect of wearing a cloth mask. The last two cases are simulated for a male younger than 30 years old. The typical computational time taken to solve one case is around 32 h with the computational resources by using 96 CPUs at the high performance computing cluster.

3. Numerical approach validation

Human cough is a perilous phenomenon and a primary pathway for spreading respiratory and air-borne diseases, as the action propels virus-bearing nuclei into the air from infectious to susceptible individuals. Human cough characterization is exceedingly complex, dependent on factors ranging from ambient temperature and RH levels to position and motion of the cougher to air turbulence, droplet size distribution, and coughing velocities. Numerical verification and validation are even more challenging due to the interaction of various underlying physical mechanisms and parameters such as turbulent dispersion, droplet collision/breakup, droplet evaporation, non-evaporative components such as DNA, lipid proteins and solid residues, particle–air interactions, particle size distribution, buoyancy forces, and numerical limitations. Furthermore, there are many uncertainties and discrepancies in the literature in terms of particle size distribution, coughing velocity profiles, coughing angles, and many environmental factors. It is important to know that the oversimplification of any of these parameters can lead to inaccurate results and conclusions, which can have significant public health effects if these are used to guide policy-making. Therefore, it is crucial to verify and validate the numerical methodology and results with experimental and analytical predictions for coughing dynamics.

The experimental and analytical model data from Bourouiba et al. [21] has been used to validate Computational Fluid Dynamics (CFD) results presented in this study. They conducted a combined experimental and theoretical investigation of the violent respiratory events such as coughing and sneezing. They also observed that these events led to the formation of multiphase turbulent buoyant clouds with suspended droplets of various size distributions. In such simulations, a discrete or continuous fall out model can be used to account for the behavior of suspended droplets. In the discrete fallout model, the droplets are assumed to remain suspended in the cloud until their Stokes settling speed converges to that of the decelerating cloud which can lead to inaccurate results. On the other hand, the continuous fallout model is more accurate which based on sedimentation theory in turbulent fluids [21]. The theoretical model developed using the continuous fallout theory for the interaction between pathogen-bearing droplets and a turbulent buoyant cloud in terms of droplet fallout, and contamination range had already been verified and validated using experimental results. Therefore, for the validation part of this study, the numerical are based on all the operational conditions and physical models from Bourouiba et al. [21] for validation purposes. The droplets are assumed to be monodispersed in order to be consistent with the experiments and the theoretical model, which did not account for evaporation effects.

The literature on coughing dynamics posits that the coughing cloud advances from the source, while the puff almost retains the same shape, and its lateral extent expands linearly with distance as illustrated in Fig. 3. Moreover, the turbulent plume theory has been shown to adequately predict critical features of the violent expiratory events seen in coughing dynamics [21].

Fig. 3 shows the physical depiction of the progression of a cough cloud emitted horizontally. Negatively buoyant droplets are dispersed until they separate from the cloud at a horizontal distance (fall out length) and fall off at a final reach (contamination range). The coughing cloud, consisting of very small droplets (<10 [μm]), rises due to an increase in buoyancy forces when the negatively buoyant particles fall.

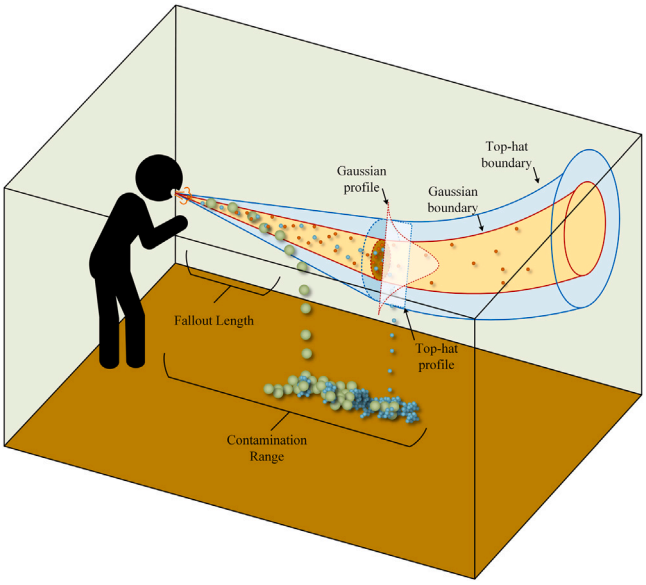

Fig. 3. Schematic of the coughing dynamics including the turbulent jet theory and contamination range definition.

Table 2
Parameters used for numerical validation of cough dynamics [21].

Parameter	Literature data
Coughing velocity [m/s]	11.2
Duration [ms]	300
Coughing angle [°]	0.0
Mouth opening [cm^2]	3.4
Human body surface temperature [°C]	37
Ambient temperature [°C]	23
Droplets and air temperature from mouth [°C]	35
Ambient RH [%]	19
Mouth relative humidity [%]	85
Particle size range [μm]	30–700

It should also be noted that the clouds are initially momentum-driven multiphase flow that transitions to buoyancy-driven mode once the net coughing velocity vanishes. Therefore, the evolution of the trajectory of the puff depends on both time-dependent momentum and buoyancy forces as predicted in the theoretical equations. Bourouiba et al.'s [21] combined experimental results and theoretical study have shown the behavior of suspended particles within the turbulent clouds, and how their ranges can be estimated. Coughing conditions such as initial velocity, mouth opening area and angle, RH, particle sizes, and other parameters from the literature were used to simulate the experimental and theoretical model results [21] as shown in Table 2.

Simulations are performed using the CFD solver StarCCM (V 15.02) considering the parameters shown in Table 2. The analytical predictions of fallout length (the horizontal distance at which the particles tend to separate from the cloud) and contamination range (horizontal deposition distance from the cougher) are compared with CFD predictions as shown in Fig. 4. The mass-weighted/particle count-weighted average distance is used to estimate the contamination range due to the scattered nature of droplet distribution on the ground. From Fig. 4, the simulation results are used to estimate the fallout and contamination ranges especially for smaller droplet sizes (<50 [μm]). For instance, droplets with an approximate size of 100 [μm] would only reach less than 1 [m] from the cougher, whereas droplets less than 30 [μm] could reach about 2.4 [m]. Furthermore, ejection of large particles (greater than 300 [μm]) could extend the contamination range significantly, which is consistent with the predictions by Bourouiba et al. [21]. Fig. 5 shows the trajectories of two multiphase buoyant clouds for the

Table 3
List of all the simulation cases evaluated in this study. M and F represent *Male* and *Female*, whereas w/o stands for *without*.

Case No.	Posture	Gender	Age-group	Ventilation	Mask
1	Standing	M	<30	AC	w/o Mask
2	Standing	M	30–50	AC	w/o Mask
3	Standing	M	>50	AC	w/o Mask
4	Standing	F	<30	AC	w/o Mask
5	Standing	F	30–50	AC	w/o Mask
6	Standing	F	>50	AC	w/o Mask
7	Sitting	M	<30	AC	w/o Mask
8	Sitting	M	30–50	AC	w/o Mask
9	Sitting	M	>50	AC	w/o Mask
10	Sitting	F	<30	AC	w/o Mask
11	Sitting	F	30–50	AC	w/o Mask
12	Sitting	F	>50	AC	w/o Mask
13	Standing	M	<30	No AC	w/o Mask
14	Standing	M	<30	No AC	with Mask
15	Standing	M	<30	AC	with Mask

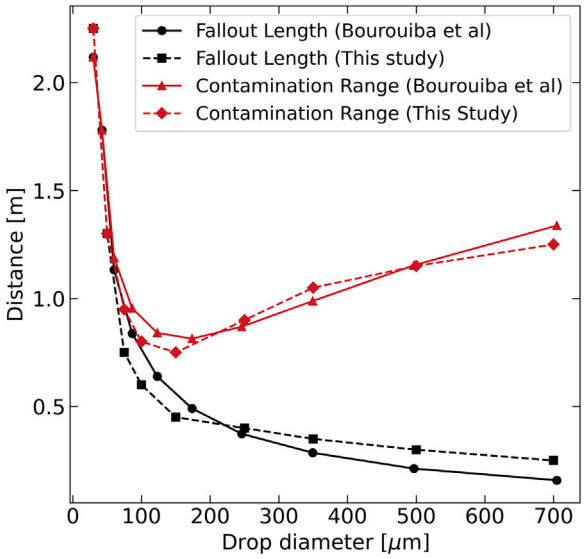

Fig. 4. Fall out distance (black color) and contamination range (red color) as predicted by this study (dashed) compared to the theoretical study by Bourouiba et al. [21] (solid).

monodispersed particle sizes of 700 [μm] and 30 [μm], as predicted by the theoretical models [21] and CFD simulations. It can be noted that the height reached by the 30 [μm] droplets is much higher (4 to 6 [m]) compared to the 700 [μm] droplets. This is due to the greater tendency to stay afloat because of the relatively higher buoyancy forces acting on them. From Figs. 4 and 5, it can be observed that the results are in good agreement for both parameters, which is crucial in estimating the contamination range accurately for a coughing event.

4. Results and discussion

The Results and Discussion section is divided into two parts. The first part shows qualitative results for cough dynamics. The second part shows quantitative results obtained through numerical simulations. In both parts, numerical simulations were used to obtained accurate results.

4.1. Qualitative cough dynamics

Fig. 6 shows the evolution of cough particles and spread of the particles for 30 [s] after the cough initiation in an air-conditioned room. The movement of cough particles is shown at six different instances

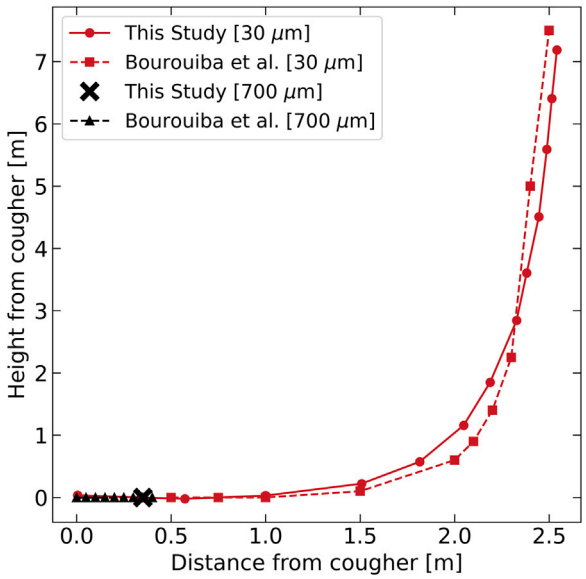

Fig. 5. Vertical fall out as predicted by this study compared to the theoretical study by Bourouiba et al. [21] for the diameter sizes of 30 [μm] and 700 [μm].

during this period. Fig. 6(a) shows the initial reach of the particles at 1 [s] immediately after the cough. The momentum of the cough carries the particles forward, up to distances greater than 2 [m]. As time progresses, the cloud loses momentum and is dominated by the external influence of air current in the room in addition to buoyancy forces acting on the particles, as seen in Fig. 6(b). Heavier particles start to fall while lighter, smaller particles start rising. A clear separation of large and small particles then becomes more visible in Fig. 6(c) at 10 [s]. At 15 [s], most of the larger particles have deposited on the ground, as seen in Fig. 6(d). Smaller particles are pushed towards the outlet vent of the room by the air conditioning system. As Figs. 6(b), 6(e), and 6(f) show, a large cluster of smaller particles can be seen close to the outlet. In Figs. 6(e) and 6(f) few larger particles are formed by coalescence of smaller particles that can be observed close to the outlet vent. At around 30 [s], aerosol particles of diameters less than 5 [μm] are detected, which stay afloat inside the room for a longer time period before they fall off or are removed by the exhaust ventilation systems. For additional information on the effect of flow field on the particle dispersion and vice versa, the reader is referred to the Appendix B.

The evolution of cough of a male sitting in an air-conditioned room is shown in Fig. 7. Particle dispersion immediately after the cough in sitting position is similar to the standing position, as shown in Fig. 7(a). After the elapse of 30 [s], lighter particles are clustered around the outlet vent and heavier particles fall to the ground, as shown in Fig. 7(b). In the sitting case, there is lesser influence of the inlet duct velocity on the cough cloud. This is because the relative distance of the mouth from the inlet duct is higher as compared to the standing case. As a consequence, the cough cloud is less perturbed by the AC system, which results in more dispersion in different directions, as shown in Fig. 8.

Spread of cough particles can be compared in a room with and without air conditioning (AC) ventilation system. Figs. 8(a) and 8(b) show the top view of the spread with and without AC, respectively. As discussed previously, smaller particles gradually move towards the outlet vent, while larger particles fall to the ground. For this particular configuration of the cougher, the presence of the AC system affects the lateral cough spread. Flow from the inlet vent, right above the coughing person, strikes the particle cloud, forcing them to spread and deposit in lateral directions of the cloud. This can be seen in Fig. 8(a), with particle spreading to the left and the right of the coughing person. With no AC inlet vent velocity, the cough particles are affected mainly by gravity and buoyancy forces. Since there is no external flow acting upon them, the spread occurs mostly in the streamwise direction of the cougher, as shown in Fig. 8(b). In addition, we investigated the effect of AC exit position on the spread of aerosolized particles in the room by doubling the distance from the coughing person to the AC exit (8 [m]). Under the given room arrangement as shown in the Appendix C, we observed negligible effect of the positioning of AC exit on the overall contamination range.

Efficacy of a face mask in a room without AC is also investigated. For this setup, Figs. 9(a) and 9(c) show the spread of cough particles in a room without a mask. Most of the spread is in the direction of the cough, and a significant number of particles remain in the proximity of the coughing person. Spread of cough particles in a similar room with a cloth mask is shown in Figs. 9(b) and 9(d). After 30 [s] of the initiation of cough, it can be seen that spread in the direction of the cough is significantly reduced, with most of the particles not going beyond 2 [m]. Moreover, most particles remain close to the coughing person while most of the smaller particles move to the top of the room. This result is in agreement with the World Health Organization guidelines of maintaining 1 [m] social distancing indoors when masks are worn [49]. However, a prolonged exposure within this 2 [m] distance may lead to the transmission of COVID-19 carrying particles due to the formation and stagnation of aerosolized coughing cloud. In a nutshell, wearing masks is essential in minimizing the risk of transmission within confined spaces.

4.2. Quantitative coughing dynamics

The following subsections include quantitative results obtained through numerical simulations. As the results show, use of masks and the position of the cougher affect the dispersion characteristics of a coughing cloud.

4.2.1. Average contamination range and maximum-reach

In order to inform public policy on social distancing guidelines, it is important to measure the dispersion of coughing particles. This is quantified using the average contamination range and maximum-reach of the droplets. The weighted average contamination range is defined as follows:

$$CR = \frac{\sum_{i=0}^{n} x_i d_i}{\sum_{i=0}^{n} x_i} \tag{10}$$

where x_i is the particle mass or particle count and d_i is the distance traveled by the particle in the streamwise direction from the mouth.

During the transportation period, droplet could collide, resulting in coalescence, or bounce off. They could also break up due to high slip velocity or acceleration of the particles. Furthermore, droplet evaporation could occur as well, based on the Sherwood number of the droplet. All of the afore-mentioned effects were included in the simulation setup. While all three phenomena were observed in the results, particle coalescence was the most evident. Droplets that came out of the mouth ranged in size between 0.3 [μm] and 55 [μm], while at the end of 30 [s] period, droplets with diameters up to 220 [μm] were observed. We hypothesize that the particle mass-weighted CR is influenced by the large size (higher mass) particles, whereas the particle count-weighted CR is impacted by the smallest size particles, as they are higher in numbers. Hence, the CR is calculated using both particle mass and particle count weighted average to understand its sensitivity to both these metrics. The maximum-reach of the particles is the furthest distance a droplet deposited in the direction of the cough from the origin (mouth). Another measure of quantifying the contamination spread is by estimating the percentage of the particles within a certain distance from the coughing person. Therefore, two thresholds of 2 [m] and 3 [m] have been used to estimate the percentage of particles deposited on the ground within the prescribed distance.

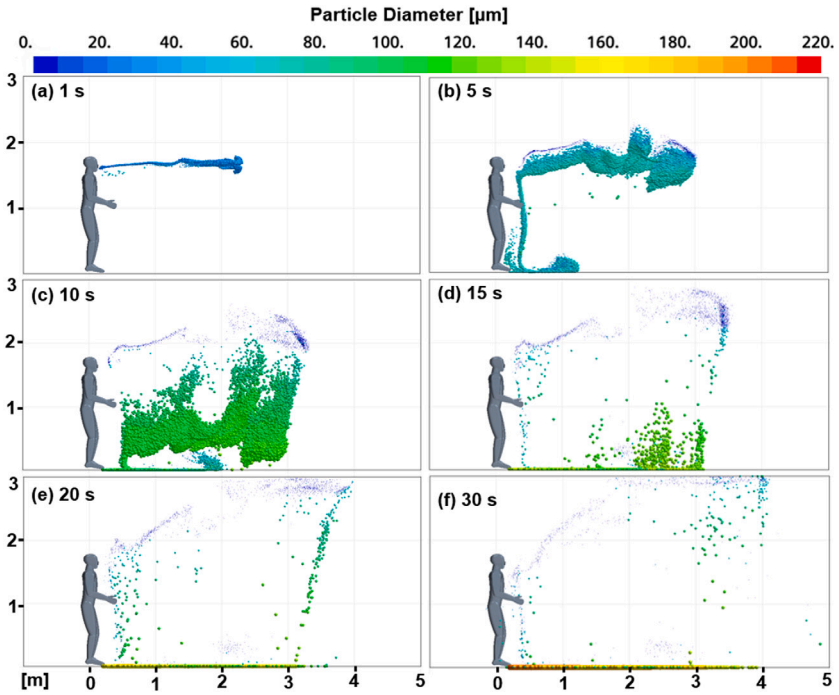

Fig. 6. Evolution of a cough cloud in standing condition at (a) 1 [s], (b) 5 [s], (c) 10 [s], (d) 15 [s], (e) 20 [s], 30 [s] after the cough for the case of M < 30.

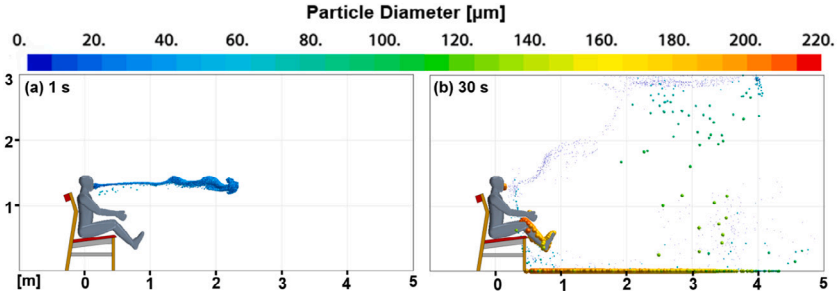

Fig. 7. Evolution of cough in sitting condition at (a) 1 [s] and (b) 30 [s] of M < 30 in an air-conditioned room.

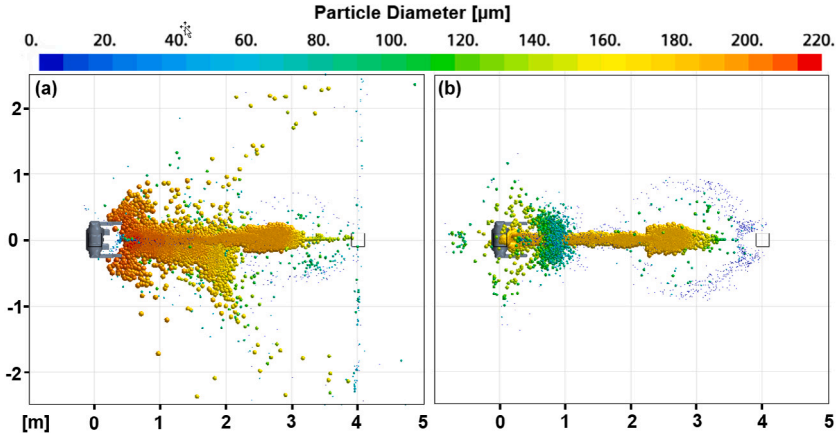

Fig. 8. The spread of cough particles for standing position in (a) an air-conditioned room vs (b) a room without an air-conditioning system at 30 [s].

Contamination range and the maximum-reach of cough particles under the AC condition for different age groups of males in sitting and standing positions are shown in Fig. 10. Contamination by a single cough is shown in the sitting and standing positions for each age group (Fig. 10). It can be noted that both types of contamination range calculations produce similar values for sitting and standing positions. Among males, the contamination range does not vary significantly with age and position.

Maximum-reach of cough particles in the standing position for age group M > 50 is highest, followed by M < 30 and then M 30–50. This trend can be attributed to a similar pattern in the number of particles emitted by each age group during a single cough. In the sitting position,

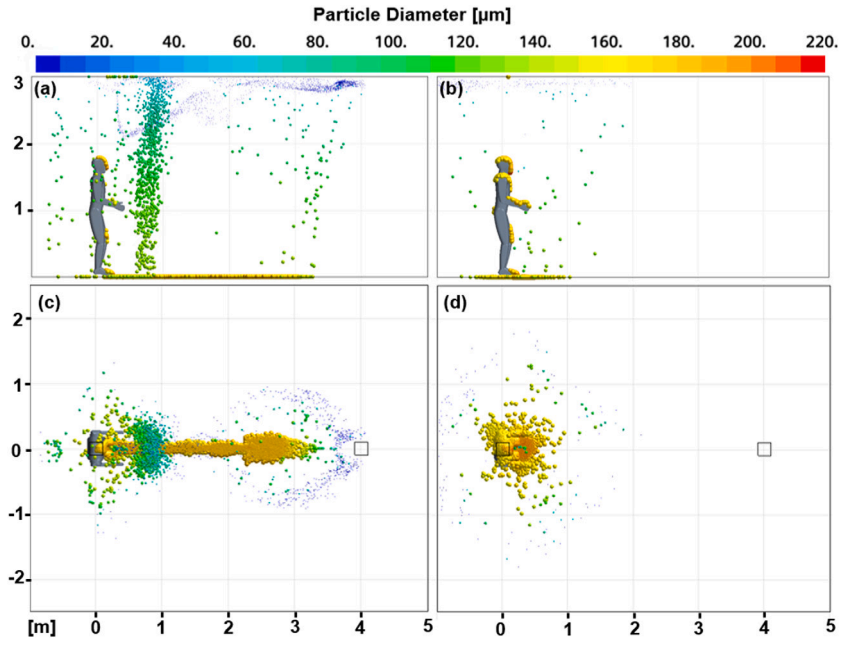

Fig. 9. The efficacy of cloth mask on the spread of cough particles without the AC condition at 30 [s]. (a) side view and (c) top view are cases without the face mask, whereas (b) side view and (d) top view are cases with the face mask.

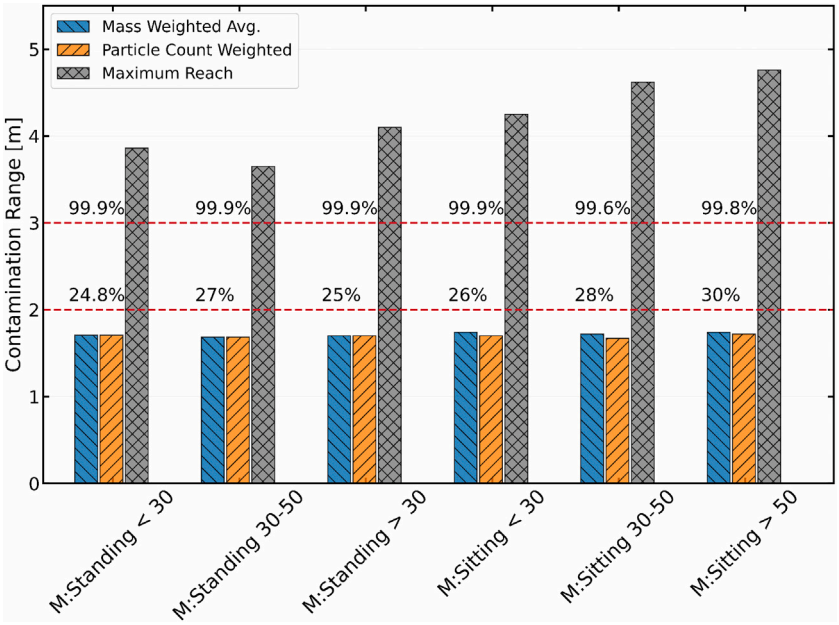

Fig. 10. Comparison of maximum-reach and contamination range of cough particles for males of different age groups in standing and sitting position with AC condition. Here, the mass-weighted average contamination range, particle-weighted average contamination range, and maximum-reach metrics are compared for different cases.

it can be observed that the particles reach greater streamwise distances. This can be due to the lesser effect of AC duct inlet velocity as the sitting position is at a lower elevation from the duct than in the standing cases. Fig. 10 shows that about 25 to 30% of the particles are deposited within the 2 [m] threshold, whereas almost 99.9% particles are deposited within 3 [m]. Only a few number of particles reach beyond the 3 [m] distance.

The contamination range and maximum-reach values for females are shown in Fig. 11. Compared to males in similar age groups, females have a lower contamination range and maximum-reach. This can be attributed to the lower cough velocities of females compared to males. Particle count-weighted contamination range values are slightly lower than particle mass values, as seen among males.

Among females, the contamination range is quite similar in the standing position regardless of age. Maximum-reach values follow the trend of the number of particles emitted by the group during a cough event. Similar behavior is observed in male coughers as well. The contamination range values for females in the sitting position are slightly higher than in the standing position, as seen in males. In the sitting position, it is evident that the supply duct flow loses some of its momentum by the time it reaches the cough cloud, and as a result, it has a reduced effect on the cough particles, allowing them to spread more. This effect also occurs in male coughers but is not as pronounced due to their relatively high coughing velocity as compared to females.

Maximum-reach of the cough particles can be seen as slightly higher in the sitting position, for all age groups, as compared to the standing

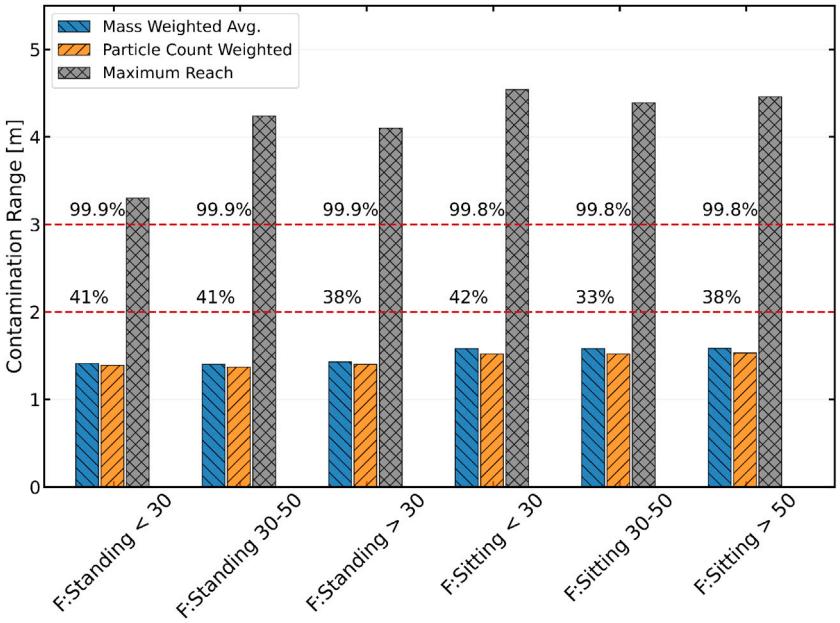

Fig. 11. Comparison of maximum-reach and contamination range of cough particles for females of different age groups in standing and sitting position with AC condition. Here, the mass-weighted average contamination range, particle-weighted average contamination range, and maximum-reach metrics are compared for different cases.

position, similar to males. However, Fig. 11 shows that about 33 to 42% of the particles are deposited within the 2 [m] threshold, whereas almost 99.9% particles are deposited within 3 [m]. A higher percentage of particles are deposited for female age groups within the 2 [m] threshold than the different male age groups due to lower coughing velocity among females.

To study the efficacy of the cloth mask, and the effect of AC ventilation on the spread of cough particles, a representative case of M < 30 in the standing position was simulated with the conditions; (i) No AC, without mask, (ii) No AC, with mask, (iii) AC, without mask, and (iv) AC, with mask.

Maximum-reach and contamination range of these four cases are compared in Fig. 12. The No AC, without mask shows the cough simulation results with AC off, i.e., no influence of inlet vent velocity. Comparing this case to the AC, without mask, the contamination range remains approximately the same; however, the maximum-reach is lower once the AC ventilation is turned off. This is expected, as turning off the AC airflow would allow buoyancy forces on the particles to have a predominant role, moving lighter particles upwards, almost vertically, resulting in lower particle spread. The No AC, with mask case in Fig. 12 shows the condition, which includes a mask with the AC ventilation turned off. This case shows minimum values for maximum-reach and contamination range. The average contamination range is close to 0.5 [m], which is in line with the Center for Disease Control and Prevention [2] and World Health Organization [49] guidelines, and the maximum-reach of the particles is just over 2 [m]. This shows the efficacy of wearing cloth mask in limiting the spread of particles assuming no external flow sources. The AC, without mask case has the highest contamination range and maximum-reach, making it the worst-case scenario among the cases shown in Fig. 12. Finally, AC, with mask case in Fig. 12 shows the coughing results in a room with the AC ventilation on, while the coughing person is wearing a mask. Compared to the case with AC ventilation being turned off, the maximum-reach and the contamination range of the particle increases. The inlet duct velocity continues to cause flow disturbance in the cough cloud, spreading the particles further away. The maximum-reach of particles is about 3.8 [m], which is almost four times the reach of the particles without AC ventilation while wearing a cloth mask. Another way of looking at the efficacy of wearing masks is by comparing the number of particles deposited up to 2 [m] and 3 [m] thresholds. Almost 99.6% of the particles are deposited within a 2 [m] distance from the coughing person in this case (AC, with mask). In contrast, only about 25% of the particles are deposited within a 2 [m] distance without wearing the mask. Similar behavior can be observed for the cases without AC ventilation as well. From these results, it can be stated that the 2 [m] social distancing guidelines are applicable only when masks are worn. Even though when wearing masks, external flow sources, such as intake/exhaust air streams and other ventilation system features, may result in a small percentage (<0.5%) of particles reaching distances beyond 2 [m].

4.2.2. Particle reach probability (PRP)

After a violent expiratory event such as coughing, different size of particles are emitted into the surrounding environment. Depending on their size, velocity, and mass and momentum interaction with the surrounding flow field, they are dispersed in the medium differently; with larger particles mostly being deposited on the ground within a short distance. To formally quantify this behavior, the concept of PRP is introduced. For a particle of a given diameter, d_i, in the cough, the PRP can be defined as the likelihood of the particle being dispersed in the free-stream medium at a certain streamwise distance, x and time t. Mathematically this can be expressed as follows:

$$\mathrm{PRP}_i(x,t) = 1 - \frac{N_i(x,t)}{N_t} \tag{11}$$

where $\mathrm{PRP}_i(x,t)$ is the particle reach probability of the diameter d_i, $N_i(x,t)$ are cumulative number of particles deposited at x and N_t is the total number of particles. Note that the PRP is a function of relative magnitudes of N_i and N_t for a droplet of a particular diameter size instead of their absolute values. This implies that the PRP does not measure the quantity of particles reaching a certain streamwise distance.

Using Eq. (11), different scenarios involving age groups, gender, posture, air conditioning ventilation, and mask are evaluated as part of this study. From Eq. (11), it is evident that at high PRP values, most particles are still dispersed in the air whereas a PRP value of zero corresponds to a complete deposition of particles.

Fig. 13 illustrates the quantitative comparison of PRP for different age groups and postures in females. For statistical analysis purposes, the particle diameters are divided into 20 bin sizes. The PRP for all the

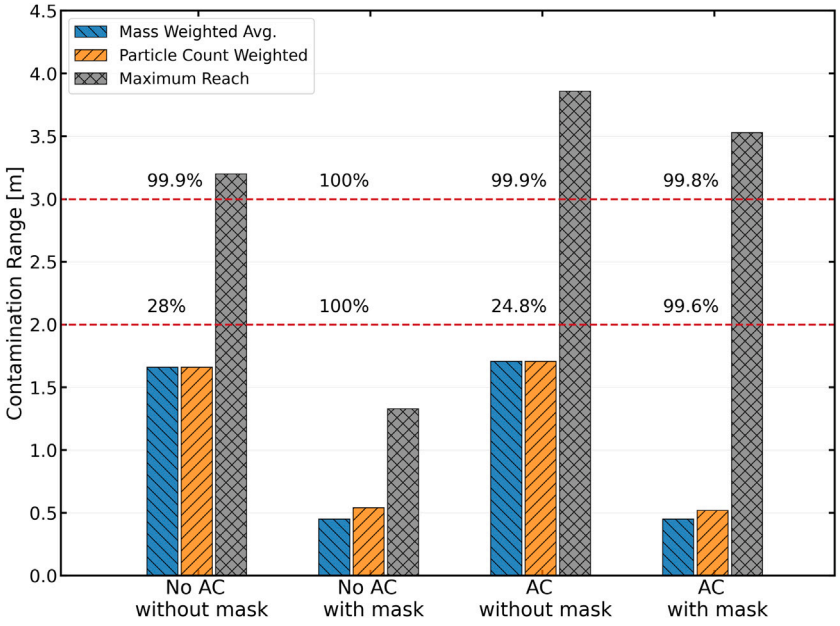

Fig. 12. Comparison of maximum-reach and contamination range of cough particles for M < 30, in standing position, coughing in a room with and without AC with and without mask. Here, the mass-weighted average contamination range, particle-weighted average contamination range, and maximum-reach metrics are compared for different cases.

size distribution was calculated, however for the sake of brevity, only three categories of key importance are presented here. The category D1, in the legend of the PRP plots, represents aerosol particles (Diameter [<5μm]). D2 covers a more intermediate range of sizes between 110–120 [μm], whereas D3 represents the largest size in the cough diameter distribution with the particle frequency of a minimum of 5000. The frequency threshold of 5000 for the largest diameter size is put in place to exclude the large particle sizes with low count. From the general trend seen in Fig. 13, it is observed that for the given streamwise distance, the PRP decreases with diameter. This implies that heavier particles tend to fall to the ground closer to the coughing subject while the lighter particles tend to stay afloat. In particular, the particle diameter in the aerosol range shows a strong tendency to stay in the air even at distances 4 [m] from the subject. Despite a slight variance for sitting versus the standing case, this tendency is consistently high for all age groups and cases (PRP > 0.9). On the other extreme, the largest particles in the diameter distribution fall to the ground at a distance of less than 2 [m] for all age groups, sizes, and postures. Small variations, however, are observed between the deposition length for sitting versus standing cases. Droplets in the sitting case can be observed to be deposited at a distance slightly farther than in the standing cases. This can be attributed to the fact that the flow field from the air-conditioner affects the heavier particles more due to its proximity in the standing position. Hence, heavier particles in that position fall to the ground at a shorter streamwise distance, x. This assertion is also supported by the PRP plot of the intermediate diameter sizes, where a significant distance is observed in the streamwise direction at which the PRP reaches a value of zero.

The PRP distribution for different postures and age groups for the male at 30 [s] is shown in Fig. 14. Although the general trend for the PRP variations with different diameters remains the same as compared with the female case shown in Fig. 13, there no significant difference in the particle deposition distance for the heaviest particles in the distribution. However, in general, the PRP is observed to be slightly higher for the male cases. This can be attributed to the higher peak coughing velocities for males as compared to females. For the male case, slight differences were observed between the postures with the trend similar to that discussed for the female case; however, no significant disparity was observed in the PRP for different age groups.

Figs. 13 and 14 depict no significant differences in the PRP of aerosols for different postures, age groups, and gender. Since aerosols (particle sizes < 10 [μm]) are the critical transmission carriers for airborne contamination, it is essential to pay close attention towards scenarios that would reduce the airborne transmission. Fig. 15 shows the PRP plots at 30 [s] for four different scenarios including cases with and without masks and with and without air conditioning ventilation. These cases are simulated using the coughing velocity and diameter distribution of M < 30 scenario.

Several observations can be made by comparing Figs. 15 (a) and 15 (b), which illustrate the effect of ventilation on PRP in the absence of mask. For instance, the particle deposition distance increases almost 300% for the D3 category in the case without ventilation. Furthermore, a significant increase is observed in PRP for aerosols and intermediate-sized particles for the case without ventilation too, thus clearly depicting the increased risk of airborne transmission when no ventilation is available.

Figs. 15 (c) and 15 (d) shows the effects of wearing a cloth mask. It is pertinent to mention here that PRP quantifies the probability of a cough particle with the size d_i reaching the streamwise distance x regardless of the quantity of d_i at the same distance, x. The results clearly show that the effectiveness of wearing a cloth mask coupled with the AC ventilation can result in a significant reduction in the PRP for all diameter sizes, including aerosols. Consequently, this significantly reduces the risk of inhaling infectious particles at any given streamwise distance, x, from the transmitter. Out of all the four cases evaluated, the efficacy of masks combined with AC ventilation is the highest in terms of the PRP.

5. Conclusions

In this study, the complex phenomena of coughing dynamics were successfully simulated, by accounting for turbulent buoyant cloud formation and propagation, particle size distribution, particle–fluid interaction, particle coalescence/breakup, multi-component droplet evaporation, and relative humidity. Numerical results presented in this study were validated using the experimental data and analytical models from the literature. The validated methodology was then used to conduct a parametric study for three age groups of males and females in sitting and standing positions. The use of cloth mask has also been included

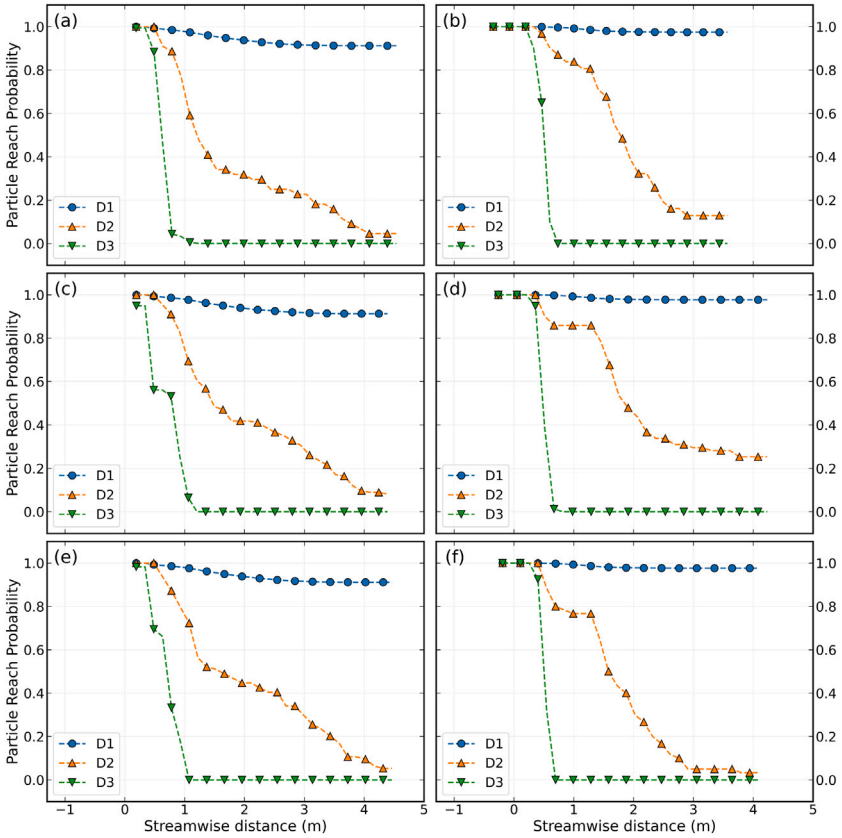

Fig. 13. Particle reach probability for different age groups and postures (females). (a) 30: Sitting, (b) 30: Standing, (c) 30–50: Sitting, (d) 30–50: Standing, (e) 50+: Sitting, and (f) 50+: Standing. D1, D2 and D3 refer to small (<5 [μm]), intermediate (110–120 [μm]), and large (>200 [μm]) particle sizes.

in the study with and without the effects of external flow. Based on the results from the study, the following conclusions can be drawn.

1. Among various age groups within each gender, there was not a significant difference in the contamination range. However, maximum-reach values for both males and females follow the trend of the number of particles emitted by each group. Compared to males in similar age groups; overall, females have a slightly lower contamination range and maximum-reach due to lower cough velocities and particle counts. Under the given room arrangement, sitting positions have a longer maximum-reach of cough particles as compared to the standing position for all age groups of males and females. This signifies that while the effect of gender on contaminant spread is marginal, the postures have a direct effect on disease transmission in confined spaces considerably.
2. The effect of air conditioning ventilation on the particle spread have been investigated in this study. In the absence of external flow, the particle spreads mainly in the streamwise direction. However, under the current air conditioning ventilation arrangement, an increased contaminant spread in the lateral direction was observed. This highlights the importance of the relative positioning of the cougher and the position of supply duct at the ceiling. On the contrary, the positioning of the AC exit had negligible effect on the contamination range.
3. Wearing a cloth mask reduces the average contamination range by approximately two-third of the distance compared to the no-mask case. Only less than 1% of particles in mask cases reached distances beyond 2 [m], as opposed to more than 70% of particles in the no-mask cases. However, the results showed that the aerosolized particles could reach further distances and stay suspended for longer periods of time (>30 [s]).
4. The PRP profiles for various cases illustrated that wearing a mask in combination with using AV ventilation can significantly reduce the particle concentration profile both for aerosols and larger droplets (>200 [μm]).

The observations highlighted above enhance our understanding of social distancing guidelines and mask efficacy in closed spaces. This work, however, can be further extended to include the effects of continuous breathing, which involves the conditions for asymptomatic spread of the viral particles. Different ventilation and air change rates could also be considered to highlight the impact of adequate ventilation on the control and mitigation of contaminant spread. Another important area of research is to study the efficacy of different types of masks in curbing aerosol transmission.

Declaration of competing interest

The authors declare that they have no known competing financial interests or personal relationships that could have appeared to influence the work reported in this paper.

Acknowledgments

The authors would like to acknowledge the High-Performance Research Computing facility of Texas A&M University for providing necessary hardware and software support. The third author would like to extend his gratitude to the Fonds de recherche du Québec - Nature et technologies (FRQNT), Canada - Bourses de doctorat (B2X). The fourth author would like to thank Fonds de recherche du Québec - Nature et technologies (FRQNT), Canada - Bourses de recherche postdoctorale (B3X). The fifth author would like to acknowledge the support of Northern Illinois University, USA. The authors are also grateful for the CAD models of the mannequin provided by Grabcad.com.

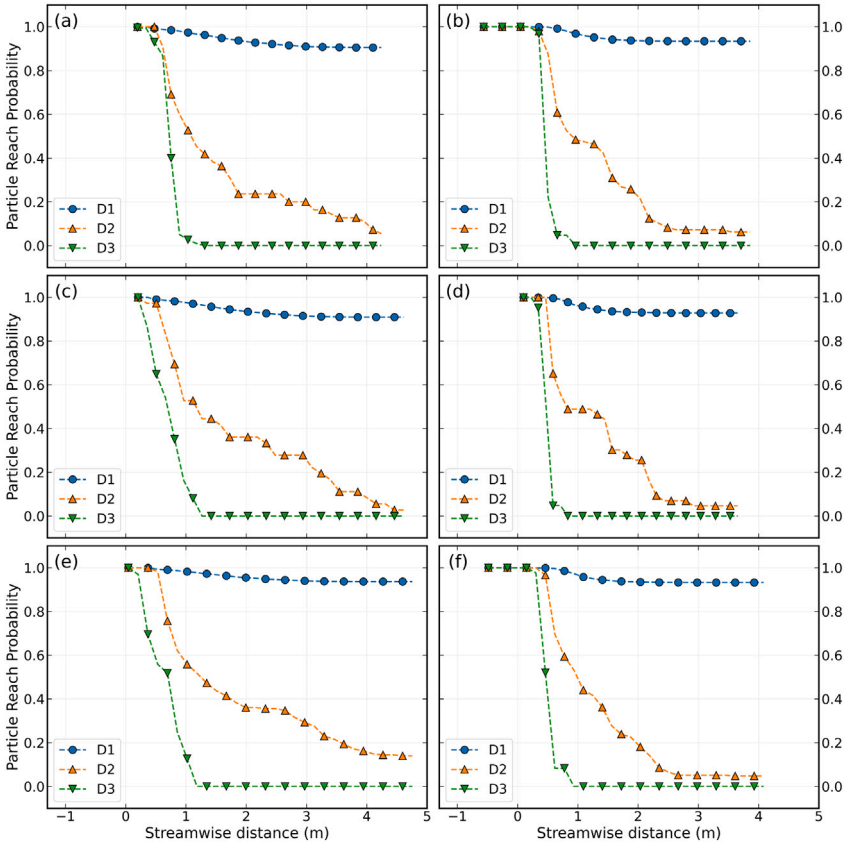

Fig. 14. Particle reach probability for different age groups and postures (males). (a) 30: Sitting, (b) 30: Standing, (c) 30–50: Sitting, (d) 30–50: Standing, (e) 50+: Sitting, and (f) 50+: Standing. D1, D2 and D3 refer to small (<5 [μm]), intermediate (110–120 [μm]), and large (>200 [μm]) particle sizes.

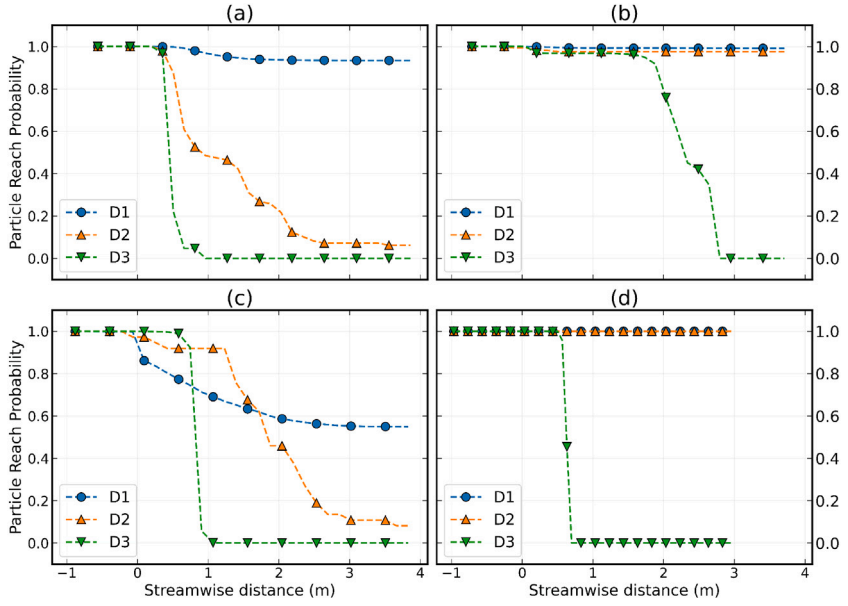

Fig. 15. Particle reach probability for M < 30 case. (a) Ventilation without mask, (b) No ventilation without mask, (c) Ventilation with mask, and (d) No ventilation with mask. D1, D2 and D3 refer to small (<5 [μm]), intermediate (110–120 [μm]), and large (>200 [μm]) particle sizes.

Appendix A. Mesh insensitivity study

Grid insensitivity study was performed to ensure the numerical results are independent of the mesh size. The center line velocity of the coughing field was selected for conducting the grid-independence check. The center line velocity across the section is measured from the mouth through the end of room in the streamwise direction at 30 [s] as shown in Fig. A.16. The overall computational domain, comprising of the mannequin and the room, was meshed using an unstructured-hexahedral, cut cell mesh. The grid in the coughing cloud region

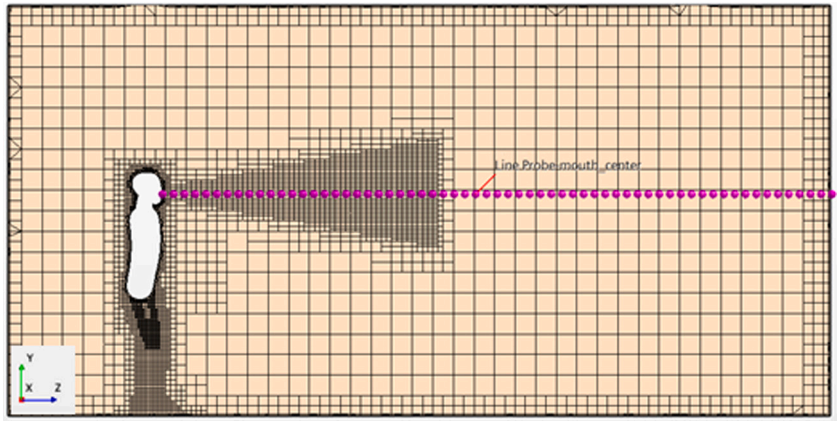

Fig. A.16. Section view of computational grid and the centerline velocity measurement probes for mesh insensitivity study.

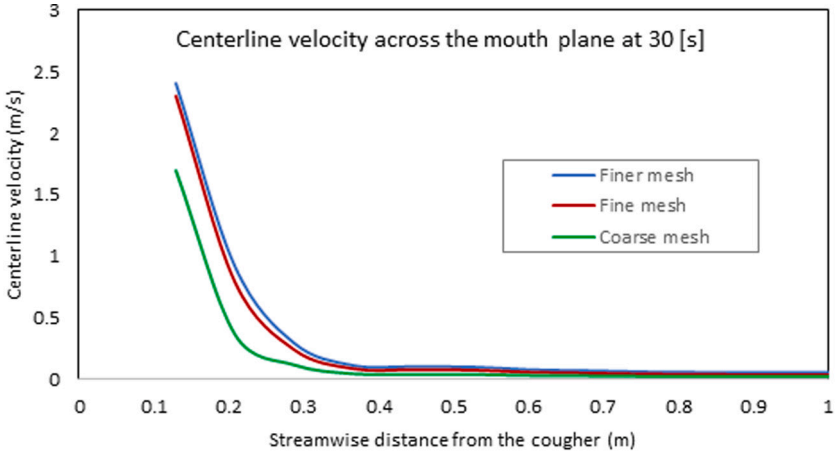

Fig. A.17. Comparison of centerline velocity predictions obtained from coarse, fine, and finer mesh sizes.

Table A.4
Different mesh sizes (coarse, fine, and finer) used for mesh insensitivity study.

Mesh	Number of elements
Coarse	143,821
Fine	288,420
Finer	577,547

as shown in Fig. A.16, was refined to capture the dynamics of the turbulent jet accurately. Three mesh sizes (coarse, fine, and finer) as shown in Table A.4 were used to compare the velocity predictions along the center line as shown Fig. A.17. It was found that the fine mesh size of 288,420 cells was a reasonable choice considering a good balance between the computational time and numerical accuracy and the same grid-sizing approach was considered for all other simulations.

Appendix B. The flow field results

Since the flow field in an AC room has a significant impact on the particle dispersion and contamination range, the line integral convolution type velocity vector field at the center section and particle map is included here. Fig. B.18 shows the effect of velocity field on the evolution of cough particles spread for up to 30 [s] after the cough initiation in an air-conditioned room. Fig. B.18(a) shows the effect of AC on initial reach of the particles at 1 [s] immediately after the cough. At 1 [s], the momentum of the cough is more dominant than the AC velocity and hence carries the particles forward, up to distances greater than 2 [m]. As time progresses, the cloud loses momentum and is dominated by the external influence of air current in the room in addition to buoyancy forces acting on the particles, as seen in Fig. B.18(b) through (f). Based on the trade-off between local velocity magnitudes and buoyancy forces, heavier particles start to fall while lighter, smaller particles start rising. It can be observed that the particle dispersion is influenced by local continuous velocity field and vice versa.

Appendix C. The effect of AC exit position

In order to study the influence of AC exit position on the contamination range, an additional simulation was run by doubling the distance from the coughing person to the AC exit (8 m). This study can also be used to understand the influence of the AC supply velocity alone. The results for the AC exit position of 4 m from the cougher is shown in Fig. 8(a) in the manuscript. The comparison of results for both 4 m and 8 m AC exit position cases are shown in Fig. C.19(a) and (b). In addition, the mass-weighted average contamination range and particle-weighted average contamination range are also post-processed for both cases and shown in Table C.5.

It can be observed that the line-along distribution near the AC exit in the 4 [m] case is not present in the 8 [m] case. However, from Fig. C.19 and Table C.5 above, the AC exit positions (4 [m] and 8 [m] from the cougher) have a negligible influence on the average contamination range under the given room arrangement. In summary, this study helped to understand the influence of AC exit position on contamination range.

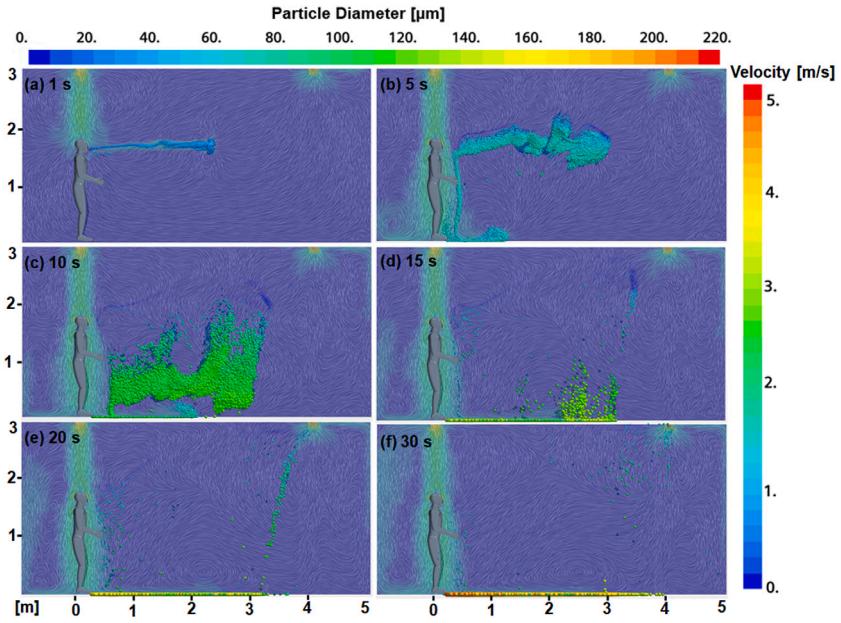

Fig. B.18. Evolution of velocity vector field and particle dispersion map at the center section.

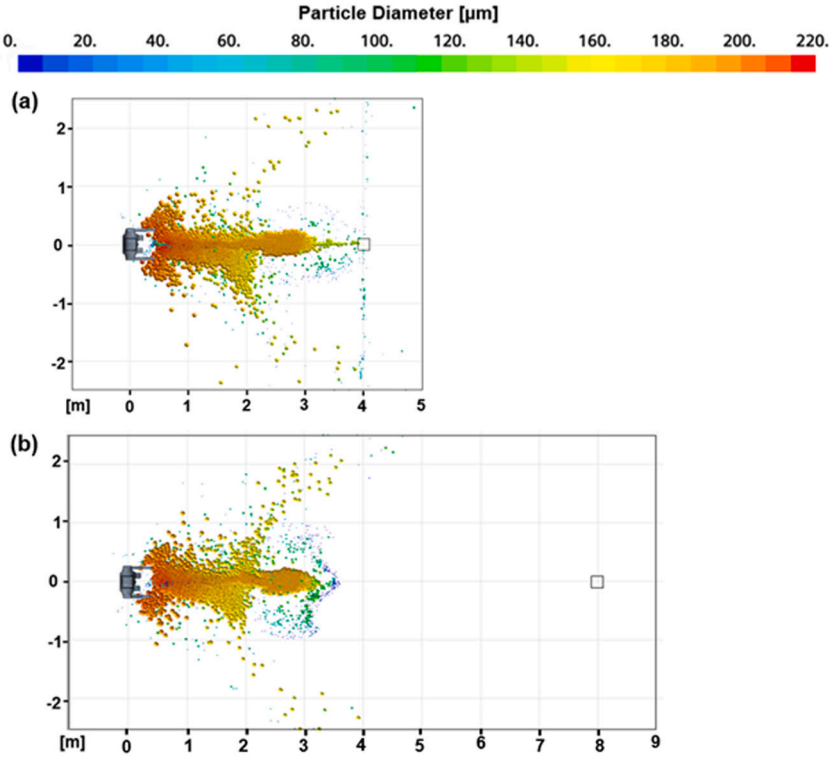

Fig. C.19. The spread of cough particles for standing position in an air-conditioned room for (a) AC position of 4 [m] and (b) 8 [m] from the coughing person at 30 [s].

Table C.5
Mass-weighted and particle-weighted average contamination range for 4 [m] and 8 [m] AC positions from the cougher.

AC Exit position	Mass-weighted average contamination range [m]	Particle-weighted average contamination range [m]
4 [m] from cougher	1.71	1.71
8 [m] from cougher	1.70	1.76

References

[1] E. Dong, H. Du, L. Gardner, An interactive web-based dashboard to track COVID-19 in real time, The Lancet Infect. Dis (ISSN: 1473-3099) 20 (5) (2020) 533–534.

[2] CDC, How COVID-19 spreads, 2020, URL https://www.cdc.gov/coronavirus/2019-ncov/prevent-getting-sick/how-covid-spreads.html.

[3] R. Zhang, Y. Li, A.L. Zhang, Y. Wang, M.J. Molina, Identifying airborne transmission as the dominant route for the spread of COVID-19, Proc. Natl. Acad. Sci. 117 (26) (2020) 14857–14863.

[4] B. Jones, P. Sharpe, C. Iddon, E.A. Hathway, C.J. Noakes, S. Fitzgerald, Modelling uncertainty in the relative risk of exposure to the SARS-CoV-2 virus by airborne aerosol transmission in well mixed indoor air, Build. Environ. 191 (2021) 107617.

[5] Z. Lau, K. Kaouri, I.M. Griffiths, Modelling airborne transmission of COVID-19 in indoor spaces using an advection-diffusion-reaction equation, 2020, arXiv preprint arXiv:2012.12267.

[6] N. Mingotti, R. Wood, C. Noakes, A.W. Woods, The mixing of airborne contaminants by the repeated passage of people along a corridor, J. Fluid Mech. 903 (2020).

[7] C.V. Vouriot, H.C. Burridge, C.J. Noakes, P.F. Linden, Seasonal variation in airborne infection risk in schools due to changes in ventilation inferred from monitored carbon dioxide, Indoor Air (2021).

[8] L. Morawska, J.W. Tang, W. Bahnfleth, P.M. Bluyssen, A. Boerstra, G. Buonanno, J. Cao, S. Dancer, A. Floto, F. Franchimon, et al., How can airborne transmission of COVID-19 indoors be minimised? Environ. Int. 142 (2020) 105832.

[9] J. Borak, Airborne transmission of COVID-19, Occup. Med. 70 (2020) 297–299.

[10] J. Redrow, S. Mao, I. Celik, J.A. Posada, Z.-g. Feng, Modeling the evaporation and dispersion of airborne sputum droplets expelled from a human cough, Build. Environ. 46 (10) (2011) 2042–2051.

[11] J. Wei, Y. Li, Enhanced spread of expiratory droplets by turbulence in a cough jet, Build. Environ. 93 (2015) 86–96.

[12] J. Duguid, The size and the duration of air-carriage of respiratory droplets and droplet-nuclei, Epidemiol. Infection 44 (6) (1946) 471–479.

[13] X. Xie, Y. Li, H. Sun, L. Liu, Exhaled droplets due to talking and coughing, J. R. Soc. Interface 6 (6) (2009) S703–S714.

[14] W.G. Lindsley, T.A. Pearce, J.B. Hudnall, K.A. Davis, S.M. Davis, M.A. Fisher, R. Khakoo, J.E. Palmer, K.E. Clark, I. Celik, C.C. Coffey, F.M. Blachere, D.H. Beezhold, Quantity and size distribution of cough-generated aerosol particles produced by influenza patients during and after illness, J. Occup. Environ. Hygiene 9 (7) (2012) 443–449.

[15] T. Dbouk, D. Drikakis, On coughing and airborne droplet transmission to humans, Phys. Fluids 32 (5) (2020) 053310.

[16] T. Dbouk, D. Drikakis, On airborne virus transmission in elevators and confined spaces, Phys. Fluids 33 (1) (2021) 011905.

[17] W. Sun, J. Ji, Transport of droplets expelled by coughing in ventilated rooms, Indoor Built Environ 16 (6) (2007) 493–504.

[18] W. Yan, Y. Zhang, Y. Sun, D. Li, Experimental and CFD study of unsteady airborne pollutant transport within an aircraft cabin mock-up, Build. Environ. 44 (1) (2009) 34–43.

[19] J.K. Gupta, C. Lin, Q. Chen, Flow dynamics and characterization of a cough, Indoor Air 19 (6) (2009) 517–525.

[20] G. Zayas, M.C. Chiang, E. Wong, F. MacDonald, C.F. Lange, A. Senthilselvan, M. King, Cough aerosol in healthy participants: Fundamental knowledge to optimize droplet-spread infectious respiratory disease management, BMC Pulm. Med 12 (1) (2012) 11.

[21] L. Bourouiba, E. Dehandschoewercker, J.W. Bush, Violent expiratory events: On coughing and sneezing, J. Fluid Mech. 745 (2014) 537–563.

[22] J.W. Tang, A. Nicolle, J. Pantelic, G.C. Koh, L. De Wang, M. Amin, C.A. Klettner, D.K. Cheong, C. Sekhar, K.W. Tham, Airflow dynamics of coughing in healthy human volunteers by shadowgraph imaging: An aid to aerosol infection control, PLoS One 7 (4) (2012).

[23] F. Liu, H. Qian, Z. Luo, S. Wang, X. Zheng, A laboratory study of the expiratory airflow and particle dispersion in the stratified indoor environment, Build. Environ. 180 (2020) 106988.

[24] B. Zhang, C. Zhu, Z. Ji, C.-H. Lin, Design and characterization of a cough simulator, J. Breath Res. 11 (1) (2017) http://dx.doi.org/10.1088/1752-7163/aa5cc6.

[25] R. Bi, A numerical investigation of human cough jet development and droplet dispersion (Master's thesis), The University of Western Ontario, 2018.

[26] R.K. Bhagat, M. Davies Wykes, S.B. Dalziel, P. Linden, Effects of ventilation on the indoor spread of COVID-19, J. Fluid Mech. 903 (2020) F1.

[27] Y. Zhang, G. Feng, Y. Bi, Y. Cai, Z. Zhang, G. Cao, Distribution of droplet aerosols generated by mouth coughing and nose breathing in an air-conditioned room, Sustainable Cities Soc. 51 (2019) 101721.

[28] S. Zhu, J.-H. Yang, S. Kato, Investigation into airborne transport characteristics of airflow due to coughing in a stagnant indoor environment, ASHRAE Trans 112 (1) (2006).

[29] W. Chen, N. Zhang, J. Wei, H.-L. Yen, Y. Li, Short-range airborne route dominates exposure of respiratory infection during close contact, Build. Environ. (2020) 106859.

[30] L. Bourouiba, Turbulent gas clouds and respiratory pathogen emissions: Potential implications for reducing transmission of COVID-19, JAMA 323 (18) (2020) 1837–1838.

[31] L. Bourouiba, The fluid dynamics of disease transmission, Annu. Rev. Fluid Mech. 53 (2021) 473–508.

[32] X. Li, Y. Shang, Y. Yan, L. Yang, J. Tu, Modelling of evaporation of cough droplets in inhomogeneous humidity fields using the multi-component Eulerian-Lagrangian approach, Build. Environ. 128 (2018) 68–76.

[33] L. Liu, J. Wei, Y. Li, A. Ooi, Evaporation and dispersion of respiratory droplets from coughing, Indoor Air 27 (1) (2017) 179–190.

[34] W. Rodi, Experience with two-layer models combining the k-epsilon model with a one-equation model near the wall, in: 29th Aerospace Sciences Meeting, 1991, p. 216.

[35] H. Nishimura, S. Sakata, A. Kaga, A new methodology for studying dynamics of aerosol particles in sneeze and cough using a digital high-vision, high-speed video system and vector analyses, PLoS One 8 (11) (2013) e80244.

[36] M. Rahiminejad, A. Haghighi, A. Dastan, O. Abouali, M. Farid, G. Ahmadi, Computer simulations of pressure and velocity fields in a human upper airway during sneezing, Comput. Biol. Med. 71 (2016) 115–127.

[37] Z. Naumann, L. Schiller, A drag coefficient correlation, Zeitschrift Des Vereines Deutscher Ingenieure 77 (318) (1935) e323.

[38] M.M. El Wakil, O. Uyehara, P. Myers, A theoretical investigation of the heating-up period of injected fuel droplets vaporizing in air, Tech. rep., University of Wisconsin–Madison, 1954.

[39] D.P. Schmidt, C. Rutland, A new droplet collision algorithm, J. Comput. Phys. 164 (1) (2000) 62–80.

[40] J.C. Beale, R.D. Reitz, Modeling spray atomization with the Kelvin-Helmholtz/Rayleigh-Taylor hybrid model, At. Sprays 9 (6) (1999).

[41] D. Spalding, A standard formulation of the steady convective mass transfer problem, Int. J. Heat Mass Transfer 1 (2–3) (1960) 192–207.

[42] W. Ranz, W. Marshall, Evaporation from drops, Chem. Eng. Progr. 48 (3) (1952) 141–146.

[43] C.D. Fryar, D. Kruszan-Moran, Q. Gu, C.L. Ogden, Mean body weight, weight, waist circumference, and body mass index among adults: United States, 1999–2000 through 2015–2016, National Health Statistics Reports, 122, 2018.

[44] V. Kumar, S. Nallamothu, S. Shrivastava, H. Jadeja, P. Nakod, P. Andrade, P. Doshi, G. Kumaraswamy, On the utility of cloth facemasks for controlling ejecta during respiratory events, 2020, arXiv preprint arXiv:2005.03444.

[45] ASHRAE Standards Committee, Ventilation for Acceptable Indoor Air Quality, Standard ANSI/ASHRAE 62.1-2013, American Society of Heating, Refrigerating and Air-Conditioning Engineers, 2016.

[46] ASHRAE Standards Committee, Thermal Environmental Conditions for Human Occupancy, Standard ANSI/ASHRAE 55-2017, American Society of Heating, Refrigerating and Air-Conditioning Engineers, 2017.

[47] H. Huang, J.A. Ayoub, Applicability of the forchheimer equation for non-Darcy flow in porous media, in: SPE Annual Technical Conference and Exhibition, Society of Petroleum Engineers, 2006.

[48] E. Saldaeva, Through thickness air permeability and thermal conductivity analysis for textile materials (Ph.D. thesis), University of Nottingham, 2009.

[49] WHO, Coronavirus disease (COVID-19) advice for the public, 2021, URL https://www.who.int/emergencies/diseases/novel-coronavirus-2019/advice-for-public.